JOURNAL GEOLOGICAL SOCIETY OF INDIA
Vol.75, January 2010, pp.98-109

Numerical Modeling of Flow Patterns around Subducting Slabs in a Viscoelastic Medium and its Implications in the Lithospheric Stress Analysis

NISHANT KUMAR, SHAMIK SARKAR* and NIBIR MANDAL
Indian Institute of Science Education and Research-Kolkata,
FC-6, Salt Lake, Sector III, Kolkata - 700 106
*Email: shamiksarkar@gmail.com

Abstract: This paper presents results obtained from numerical model experiments to show different patterns of mantle flow produced by lithospheric movement in subduction zones. Using finite element models, based on Maxwell rheology (relaxation time ~ 10^{11}S), we performed three types of experiments: *Type 1*, *Type 2* and *Type 3*. In Type 1 experiments, the lithospheric slab subducts into the mantle by translational movement, maintaining a constant subduction angle. The experimental results show that the flow perturbations occur in the form of vortices in the mantle wedge, irrespective of subduction rate and angle. The mantle wedge vortex is coupled with another vortex below the subducting plate, which tends to be more conspicuous with decreasing subduction rate. Type 2 experiments take into account a flexural deformation of the plate, and reveal its effect on the flow patterns. The flexural motion induces a flow in the form of spiral pattern at the slab edge. Density-controlled lithospheric flexural motion produces a secondary flow convergence zone beneath the overriding plate. In many convergent zones the subducting lithospheric plate undergoes detachment, and moves down into the mantle freely. Type 3 experiments demonstrate flow perturbations resulting from such slab detachments. Using three-dimensional models we analyze lithospheric stresses in convergent zone, and map the belts of horizontal compression and tension as a function of subduction angle.

Keywords: Plate tectonics, Convergent zones, Subduction, Maxwell rheology, Flow perturbations.

INTRODUCTION

Lithospheric subduction is a planetary process that has played a major role in the evolution of the Earth (Stern et al. 2002 and references therein). Theoretical and experimental studies suggest that this process is largely governed by buoyancy forces resulting from density differences between the lithospheric plate and the ambient mantle medium (Zhong and Gurnis, 1994; Tackley, 1996; Houseman and Gubbins, 1997; Pysklywec and Mitrovica, 1998). Understanding the buoyancy factor would perhaps resolve the issue of upper (Fukao et al. 1992, 2001; van der Hilst, 1995) versus whole (Ringwood, 1994; Davies, 1999; van der Hilst et al. 1991; Grand et al. 1997) mantle recycling process. Geophysical observations, e.g. seismic tomography, suggest that lithospheric plates can sink down into the lower mantle, which is possible only when the subducting plates remain under negative buoyancy forces (Forsyth and Uyeda, 1975; Hager, 1984; Zhong and Gurnis, 1994; Davies, 1995; Pysklywec and Ishii, 2000).

Lithospheric slab – mantle density contrast is the most crucial parameter in the buoyancy dynamics of subduction processes. Using petrological constraints, Ganguly et al. (2008) have recently presented a detailed account of the density contrast for an oceanic lithospheric slab moving downward across the transition zone. Their calculations show that the contrast is in the order of 0.04-0.05 gm/cc in the transition zone, which is somewhat less in the upper mantle. However, the slab always remains denser than the upper mantle, and thereby undergoes downward movement under negative buoyancy forces. Their analysis also demonstrates that, at a depth of 670 km a lithospheric slab can have lower density relative to the ambient mantle undergoing spinel to perovskite transition, and that the slab can achieve neutral buoyancy while traveling further down the lower mantle for a depth of 100 km. However, considering the kinetics of spinel to perovskite plus periclase transition they have suggested that the slab would always continue to subduct after reaching a depth of 670 km in response to negative buoyancy forces. This study explains well the process of slab penetration into

the lower mantle, as observed from seismic tomography.

Geophysical studies also indicate that subducting lithospheric slabs are generally mechanically stiffer than the surrounding mantle medium. Lithosphere has a viscosity about 10^1- 10^2 times that of the mantle (e.g. Pysklywec and Ishii 2000; Turcotte and Schubert, 2002; Tirone et al. 2009). Mechanically stiffer slabs thus perturb the kinematic state of its surrounding viscous mantle, as documented in similar studies on fluid mechanics (e.g. Masuda and Ando, 1988; Mandal et al. 2001). Using numerical models several workers have investigated the nature of such local disturbances under different geological conditions. For example, Pysklywec and Ishii (2000) have shown how a lithospheric plate develops flow perturbations in the lower mantle as it avalanches at the level of the transition zone. They demonstrate that slab avalanches can produce large-scale flow perturbations in the form of vortex. Subducting plates also involve thermo-mechanical interactions with the ambient materials, developing instabilities and secondary flows in the form of plumes or convection in the mantle wedge (e.g. Gerya et al. 2004). Details of this discussion are outside the scope of this paper, as it deals only with flow perturbations resulting from the mechanical interaction between lithospheric slab and mantle.

In this study we explore possible patterns of flow developed by the mechanical movement of lithospheric slabs under varied geometrical and kinematic conditions. Subducting plates may show a wide variation in their inclinations, e.g. Izu arc with plates subducting at gentle dips (~8°) and Eastern Aleutian arc with relatively steep dips (~22°) (Stern, 2002). The subduction velocity also varies over a wide range, about 4 cm/yr to 15 cm/yr (Weins and Gilbert, 1996; Ganguly et al. 2008). In this analysis we systematically study the flow perturbations as a function of subduction angle and velocity. The instantaneous kinematics of lithospheric slabs often involves flexural rotation, resulting in steepening of their dips. This can give rise to additional effects in flow disturbances around the slab (Pysklywec and Ishii, 2000; Honda, 2009). We extend our investigation to show how the nature of flow pattern can change depending upon the translation versus rotational motion of the lithospheric slab. The flexural motion was simulated by imposing either plate-across forces or density variation. Some workers have shown that the subducting part of a lithospheric plate may be detached from its horizontal counterpart on the earth surface, and move downward freely into the deeper mantle (e.g. Chemenda et al. 2000; Gerya et al. 2004). In this study we also analyze the pattern of instantaneous heterogeneous flow developed by a detached slab. All the flow analyses presented in this paper are entirely based on mechanical effect of slab movement in the mantle. These exclude other possible factors, such as thermo-mechanical effects and the role of fluid release by subducting lithospheric plates at deeper levels (Bose and Ganguly, 1995).

MODELING APPROACH

We considered an area of about 3000 km across the subduction zone, and 1600 km in depth. The slab lies above the transition zone between 410 km and 460 km (Fig.1). Geophysical evidence suggests time-dependent responses of the upper mantle to stresses, which can be approximated with a Maxwell elastico-viscous rheology (Turcotte et al.

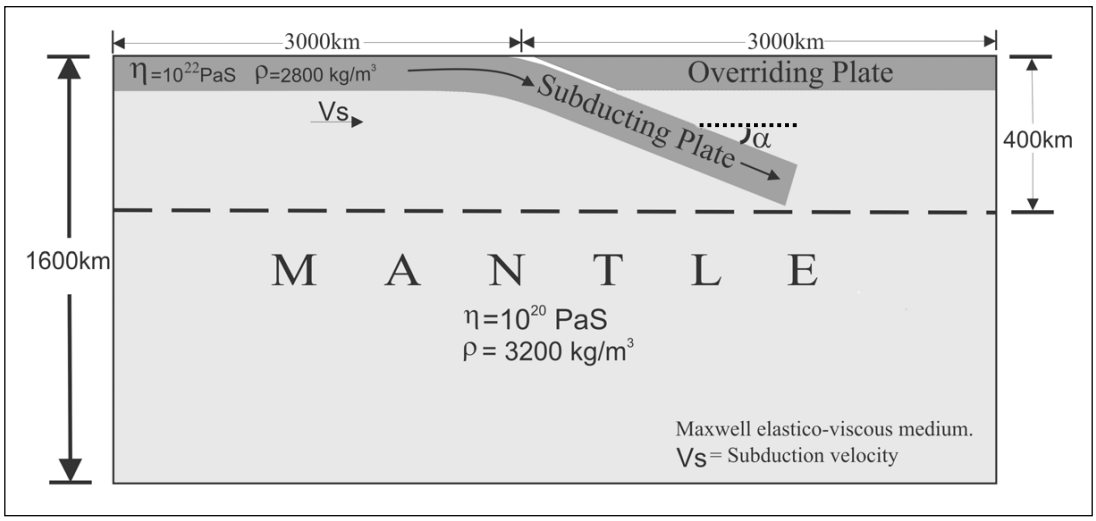

Fig.1. A schematic illustration of model considerations. V_s: subduction rate; *á*: subduction angle. Dashed line represents the initial depth of lithospheric slab considered in the model.

2004). The stress relaxation time of the upper mantle is estimated in the order of 10^{11}s. In order to develop a mechanically two-layer model, we varied the co-efficient of viscosity, keeping the shear modulus constant. The viscosity of the lithosphere was chosen 10^{22} PaS, whereas that of the underlying mantle was 10^{21} PaS. Considering isostatic equilibrium, we chose the average densities of lithosphere and mantle in the order of 2.8 and 3.2 gm/cc respectively. In some models we varied the densities both in the lithosphere and the mantle with depth. Varying density models were used to study the effects of density on the flexural bending of lithospheric plates, and in turn on the flow patterns around a subducting plate.

A 2D model consisted of three boundaries subjected to desired mechanical conditions. One of these boundaries defines the lithosphere-mantle interface with no-slip condition. The basal model boundary chosen at a depth of 1600 km is constrained kinematically, allowing no normal flow across the boundary. However, materials lying on this boundary are free to move in the horizontal direction. The transition zone is thin compared to overall vertical thickness. We therefore did not develop any separate mechanical layering, and the entire mantle region was considered to be mechanically homogeneous. In some of the models we considered the basal model boundary at a depth of 400 km, i.e. above the transition zone, to investigate flow perturbations restricted in the upper mantle. Lateral model boundaries were imposed with kinematic conditions, whereas the top one was left unrestricted (Fig.1). The subducting lithospheric plates were designed, keeping a mechanical coherence with its overlying horizontal counterpart. In some experiments we intentionally maintained an incoherent interface, allowing the subducting plate to get detached and move downward freely. We also used three-dimensional finite element to analyze lithospheric stress distributions in subduction zones as a function of subduction velocity and angle. In these models we imposed a boundary condition of no trench-parallel flow.

NUMERICAL METHOD

We employed a finite element method (FEM) for numerical model experiments. A general dynamical equation in FE computations follows:

$$m(d^2x_i/dt^2) + k\,x_i = F_i(t) \qquad (1)$$

where, m = mass matrix, k = stiffness matrix, F_i = external force vector, x_i = displacement, t = time.

In this study we used the ANSYS code (version 11, Inc. Canonsburg, PA 15317, USA) in developing the FE models. The viscoelasticity of both the lithosphere and mantle is implemented with Maxwell rheology, the representative mechanical model of which is a combination of spring and dashpot in series. Its constitutive relation follows:

$$\sigma = \int_0^t \frac{2G(t-\tau)de}{d\tau}d\tau + I\int_0^t \frac{K(t-\tau)d\Delta}{d\tau}d\tau \qquad (2)$$

where σ = Cauchy stress; e = deviatoric part of the strain; Δ = volumetric part of the strain; $G(t)$ = shear modulus as a function of time; $K(t)$ = bulk modulus as a function of time; t = current time; τ = step time and I = unit tensor. In the calculations the bulk modulus K is kept unchanged over time. On the other hand, the shear modulus undergoes a continuous change with time. The instantaneous coefficients can be determined from the following relaxation relation:

$$G(t) = (G_{ins} - G_{long})e^{-(t/\Gamma)} \qquad (3)$$

where, G_{ins} = instantaneous shear modulus, G_{long} = long term shear modulus and Γ = relaxation time, which is the most important physical parameter of Maxwell materials. Its expression follows

$$\Gamma = (\eta/G_o), \qquad (4)$$

η and G_o are the co-efficient of viscosity and the shear modulus at $t = \tau$ (eq. 2) respectively. The average values of η and G_o for the mantle are 10^{21} PaS and 10^{10} Pa, indicating the relaxation time in the order of 10^{11}S. A detailed description of the material properties chosen for numerical model experiments is given in Table 1.

We performed three types of numerical experiments using different kinematic conditions of the subducting slab. *Type 1 experiments*: the slab moves downward with a uniform velocity, maintaining a constant inclination (Fig.2a). Using Type 1 experiments we studied independently the effects of subduction rate (V_s) and angle (α) on the patterns of flow perturbations. Motion was imposed upon the plate, taking no density effects. *Type 2 experiments*: the models were designed to simulate a flexural bending in the plate (Fig.2b). In order to introduce this flexural deflection, we applied forces across the subducting slab with magnitudes increasing in the downward direction. The purpose of using Type 2 models is to investigate how a subducting plate that slows down its forward motion can perturb the flow in the mantle due to a rotational motion. We conducted similar experiments on slabs undergoing simultaneously both flexural and translational motion (Fig.2b). The flexural bending in these cases developed in response to differential imposed forces to the slab, and therefore does not directly relate to density variation, which

Table 1. Material properties and finite element parameters used for numerical experiments

Material Properties Used in the study					
	Density	Shear Modulus		Bulk Modulus	Relaxation time
		Short term	Long Term		
Lithosphere	2800 kg/m^3	2*10^{11} Pa	2*10^8 Pa	6*10^{11} Pa	1*10^{11} Pa
Mantle	3200 kg/m^3	2*10^{11} Pa	2*10^8 Pa	6*10^{11} Pa	1*10^9 Pa
Finite Element Consideration					
	No. of Nodes	Type of Element			
2D Models	3*10^4	Visco88* >> Triangular, Thermorheologically simple (TRS) viscoelastic, 2 degrees of freedom at each node.			
3D Models	2*10^5	Visco89* >> Tetrahedral, Thermorheologically simple (TRS) viscoelastic, 3 degrees of freedom at each node.			
*Elements are ANSYS® defined					

Density in mantle and lithosphere: Mantle density changes form 3200 (SI unit) to 4000 within first 500 km depth almost linearly. We have used 9 different density contours in this region as can be seen in Fig. 12a. We have kept a density of 4500 from 500 km to 1100 km and a density of 5000 from 1100 km to 1700 km depth. For the lithosphere, a density change from 2600 to 5600 is provided from the depth range of 100 km to 500 km. Data source: Lowrie, W. (2007).

is supposed to be the most crucial factor in controlling the flexural motion in subducting lithospheric plates. We designed type 2 models with a density variation in the subducting plate, giving rise to a flexural bending. Such models were developed in the following manner. The subducting plate was segmented into a number of blocks with increasing densities in the downward direction, considering either a uniform or a varying mantle density (Fig. 2b). There are uncertainties in the density profile with depth in the mantle. However, using different theoretical models geophysicists have deciphered a gross variation in density with depth (Ranalli, 1987). Based on the available data, the average crustal density is in the order of 2.4 gm/cc, which becomes more than 4 gm/cc in the lower mantle (Ganguly et al. 2008). We chose the density variation of this order in our models. *Type 3 experiments*: We used this type to investigate the nature of flow produced by a detached slab moving downward freely. This type of experiment was considered based on the hypothesis of lithospheric slab detachment in the evolution of the Himalayan-Tibet convergent system (e.g. Chemenda et al. 2000). We, however, simplified the boundary conditions for simulation of slab detachment in the models. The subducting slab was mechanically isolated from its horizontal counterpart, and subjected to forces in such a manner that the slab moved downward along its length with a uniform velocity (Fig. 2c).

EXPERIMENTAL RESULTS

Type 1 Experiments

FE models show a strongly heterogeneous flow pattern around the subducting plate (Fig.3a, b). A large-scale asymmetric vortex forms in the mantle wedge. The vortex centre is located at a depth of about 200 km. This results in a back flow (against the subduction direction) below the overriding plate. The maximum rate of back flow was estimated about one third the subduction rate, which rapidly decreased down to nearly zero at the base of the overriding plate. This strong gradient in the flow rate develops intense basal shear, resulting in stress localization in the overriding lithospheric plate (discussed in later section).

The subducting plate drags the mantle material to flow grossly along hyperbolic streamlines in the mantle region below it (Fig.3c). There is a thick boundary layer of plate-parallel flow, implying a considerable volume of mantle material recycling driven by the mechanical movement of lithospheric slabs. A strong flow divergence develops in front of the slab, forcing mantle materials to flow partly into shallow levels and partly into the deeper levels (Fig. 3c).

We ran two sets of experiments to study the effects of subduction angle (α) and rates (V_s) on the heterogeneous flow pattern. V_s and α were varied between 3 cm/yr and 16 cm/yr, and 3^o and 45^o, respectively. The flow pattern changes, both quantitatively and qualitatively, with increasing V_s. For V_s = 3 cm/yr, a flow separation occurs in the mantle wedge, forming a vortex in the shallow level (cf. Honda 2009). This is coupled with another vortex beneath the subducting plate (Fig. 4a). With increase in V_s, the vortex in the mantle wedge remains unchanged, whereas the other vortex tends to enlarge in size, and shifts its centre in the horizontal direction away from the subducting slab (Fig. 4b). For V_s = 16 cm/yr, the latter becomes strongly elliptical in shape, defining two

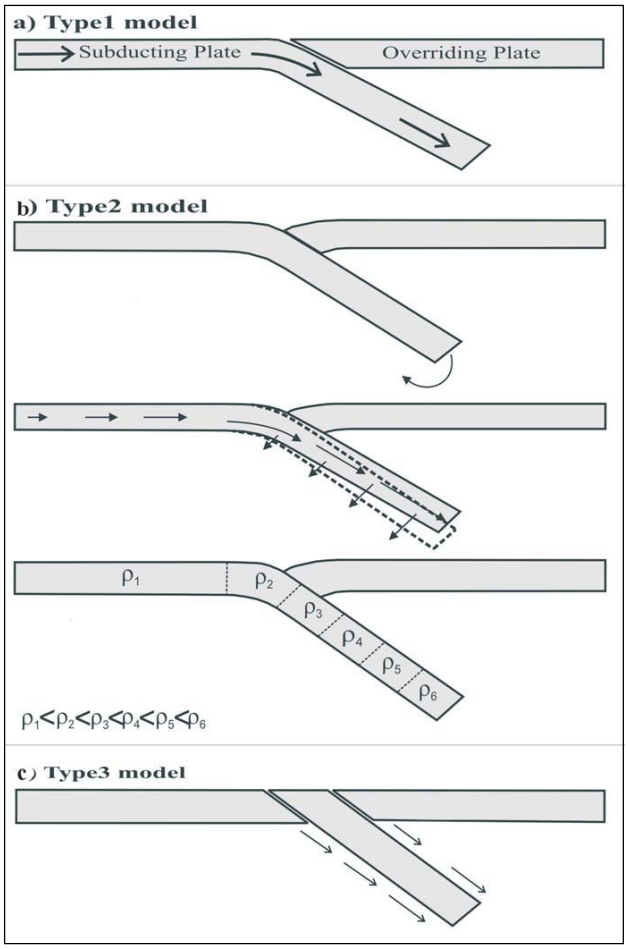

Fig.2. Three types of experiments on FE Models: **(a)** Type 1- lithospheric subduction by translation movement at a constant subduction angle. Each node in the subducting plate is subjected to a displacement vector, simulating movement of the lithosphere with a constant rate along a curvilinear trajectory. **(b)** Type 2- slabs undergoing only flexural rotation under varying lateral forces (top), movement by a combination of translation and flexure (center) and movement in presence of varying lithospheric density (bottom). **(c)** Type 3- length-parallel movement of detached slabs in mantle.

layers of forward and back flow in the shallow and deeper levels respectively. Shear localization can develop in a narrow zone between the two layers at a depth of about 300 km below the lithospheric plate (Fig. 4b). With decreasing V_s the velocity profile shows a gentle gradient, indicating gradational variation in the flow reversal (Fig. 5).

The location of flow vortex in the mantle wedge varies with subduction angle (α). For $\alpha = 10^o$, the vortex center occurs close to the tip of the subducting slab, and the vortex shape is strongly asymmetrical, resulting in flow over the entire mantle wedge (Fig. 3b). With increasing α the vortex center shifts to a shallower level, and localizes in the frontal part of the mantle wedge (Fig. 4b). The nature of flow patterns below the subducting plate also varies with α. For lower α values, these are characterized by open streamlines with hyperbolic geometry. This pattern is replaced by vortex-type geometry, as α becomes large.

Type 2 Experiments

We performed a set of experiments, simulating only flexural bending in the lithospheric plate. In this case the inclined slab underwent purely rotational motion, and steepened its dip. The flow patterns significantly differ from those in Type 1 experiments. The flexural motion of the subducting plate forces the viscous mantle material to flow with spiral trajectories at its front (Fig. 6a, b), in contrast to divergence flow in Type 1 models (Fig. 3b). This spiral

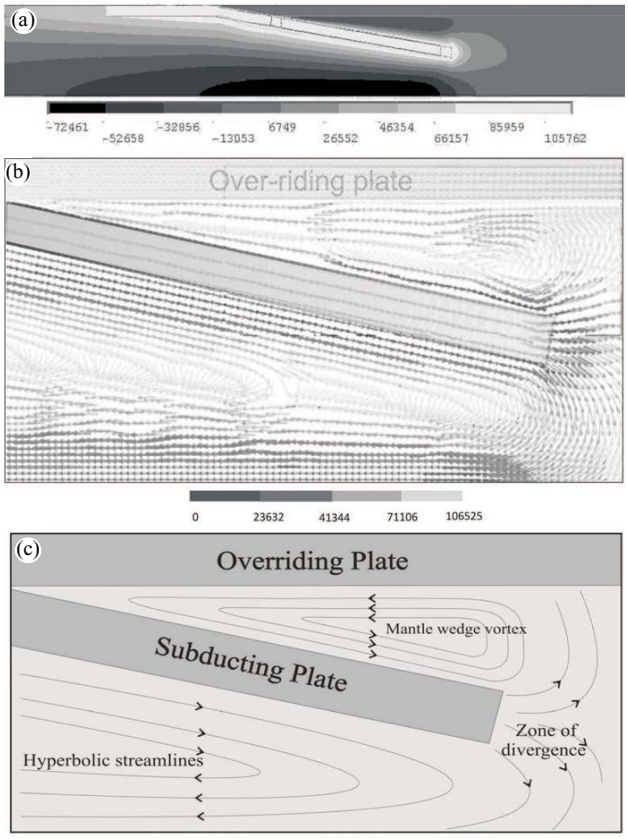

Fig.3. Flow perturbations by slab movement in Type 1 experiments. **(a)** Flow map showing variations in the magnitude of horizontal displacement components. Contours with negative values show flow against the subduction direction. **(b)** Displacement vectors showing the flow pattern around the slab. Note the presence of a distinct asymmetric vortex in the mantle wedge (shown in rectangular box). Shade contours indicate the magnitude of displacements. **(c)** Idealized streamline patterns derived from Fig.4b. Contour values are in meter.

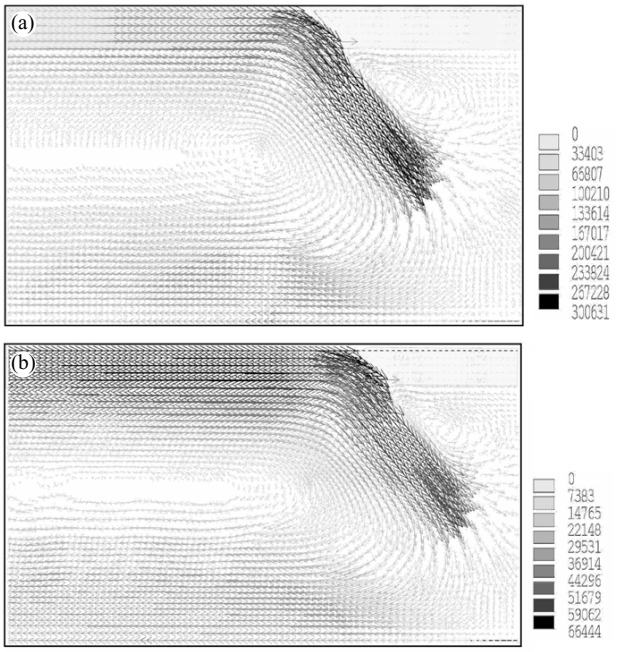

Fig.4. Controls of subduction rate (V_s) on the flow patterns in Type 1 experiments (see text for details). $\alpha = 45^o$. **(a)** V_s = 3 cm/yr and **(b)** V_s = 16 cm/yr. Arrows show displacement vectors. Numerical values of the shade bars are in SI unit.

motion eventually gives rise to a back flow in the mantle wedge. On the other hand, the mantle material beneath the subducting plate flow into deeper levels, describing curvilinear streamlines (Fig. 6b, c). The streamlines finally converge with those forming the spiral motion at the front of the subducting plate.

We ran another set of experiments with lithospheric slabs moving downward by a combination of flexural rotation and

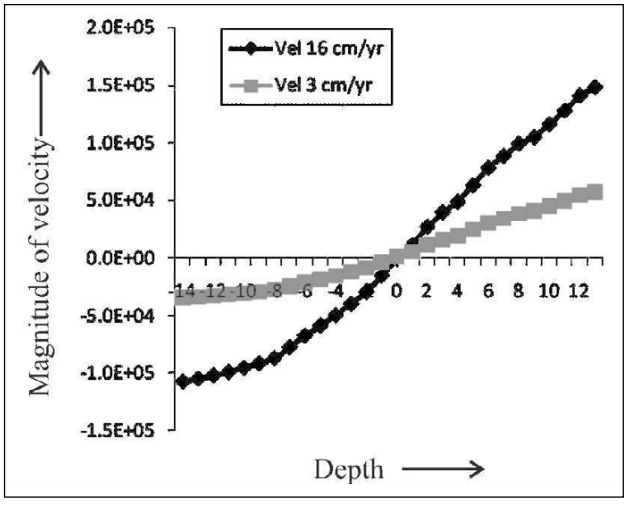

Fig.5. Effects of subduction rate on the velocity profiles on vertical sections. The sections were chosen along the central line of models.

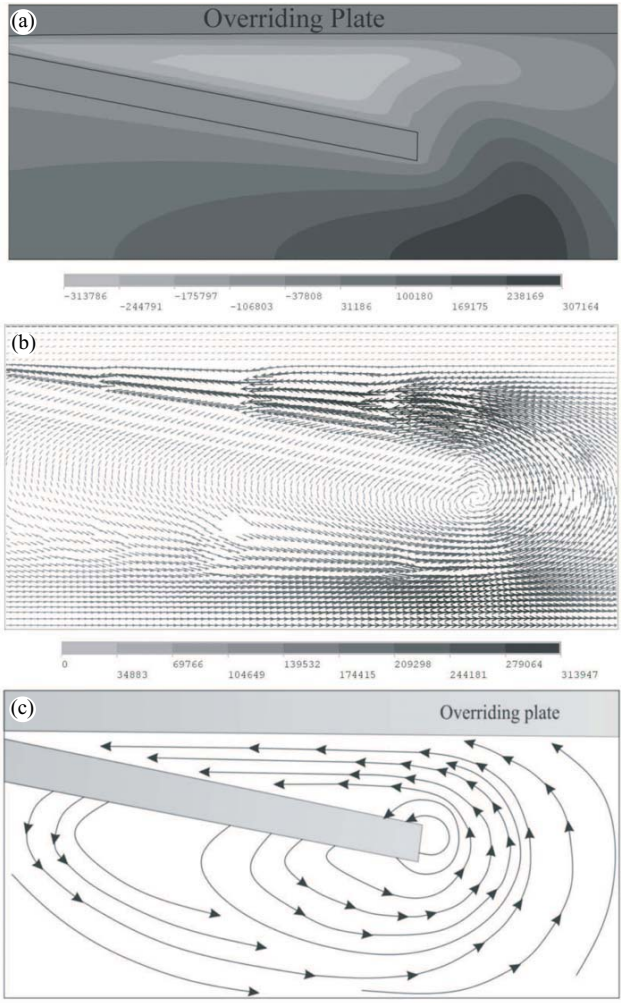

Fig.6. Flow perturbations around lithospheric slab undergoing pure flexural motion in Type 2 experiments. **(a)** Contour diagrams showing flow directions. Note that the entire mantle wedge is subjected to back flow (i.e. flow against subduction direction). **(b)** Velocity vectors describing the flow pattern. **(c)** Generalized streamlines of flow derived from Fig.6b. Numerical values of the shade bars are in SI unit.

translation. This kinematic condition also produces a large-scale spiral motion, which develops a back flow in the shallow level of the mantle wedge (Fig. 7a, b). The flow patterns beneath the subducting plate differ significantly from that in pure flexural models. Pure flexure perturbs the mantle region entirely, producing a flow in the direction of subduction. On the other hand, flow separations take place when the plate movement occurs by a combination of flexural rotation and translation. There are two flow regimes: one with back flow and the other with forward flow with streamlines conforming to that of the spiral motion (Fig. 7c).

We ran Type 2 experiments, simulating density controlled

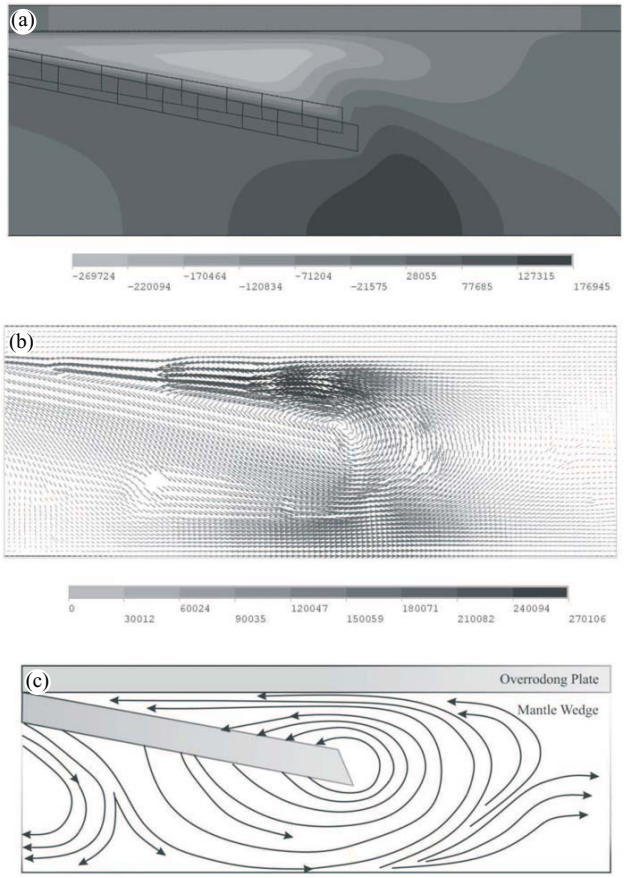

Fig.7. Type 2 experiments with lithospheric slab movement by a combination of translation and flexure. **(a)** Contours revealing horizontal displacements. **(b)** Velocity vector field. **(c)** Streamline patterns in the corresponding experiment.

flexure of the subducting plate. The mantle in these experiments was considered to have either a uniform or a varying density. Experiments show that the patterns of lithospheric flexure in the two cases are different (Fig.8). For a uniform mantle density, the flexure takes place non-uniformly, and develops sinuous geometry of the lithospheric slab. The plate deflects upward locally from its initial level (Fig.8b). However, the magnitude of upward deflection is much less compared to that in the downward direction. The latter becomes a maximum at the plate edge. In contrast, models with increasing mantle density along depth show flexural patterns resembling that of an elastic plate subjected to loading at one end (Fig.8c). We describe below the flow patterns for the two cases.

The condition of uniform mantle density produced an extremely heterogeneous flow pattern, which is characterized by a number of flow separations. The mantle wedge developed a vortex flanked by narrow zones of downward flow convergence and upward flow divergence (Fig. 9). In

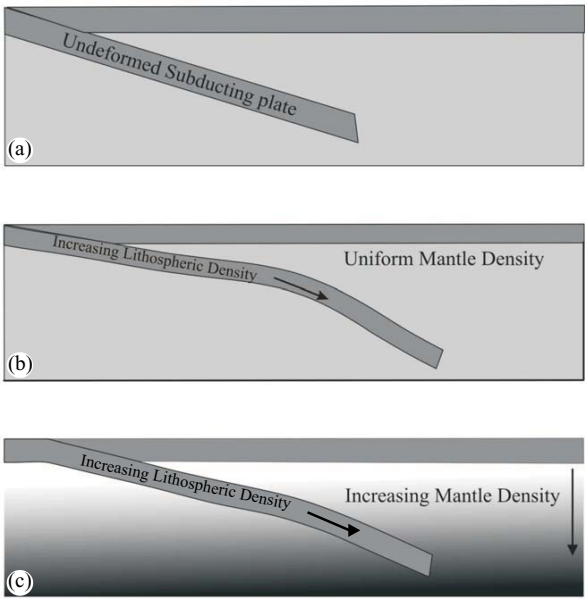

Fig.8. Density controlled flexural deformations of lithospheric plates (Type 2 model). **(a)** Initial undeformed model. **(b)** Varying density of lithospheric plate, but uniform mantle density. **(c)** Density varying both in the lithosphere and the mantle.

the mantle wedge, there is a limited extent of back flow, and the flow takes place mostly in the subduction direction, in contrast to those in previous models. The flow beneath the subducting plate also occurs in the direction of plate movement.

The flow patterns in models with varying mantle density differ significantly from that described above (Fig. 10a). Vortex-like flow is characteristically absent, and a secondary flow convergence occurs in the mantle wedge (Fig. 10b). Materials beneath the subducting plate flow mostly vertically into deeper levels.

Type 3 Experiments

Experiments show that a detached lithospheric slab develops a pair of flow vortices on either side of it (Fig. 11). The vortices are disposed symmetrically, but with opposite senses of circulation. With decrease in subduction angle, the flow vortex lying above the subducting plate tends to weaken, whereas that lying below the plate spreads laterally. Furthermore, the horizontal separation of the vortices becomes wider, and their shapes tend to become more asymmetrical with decreasing inclination of the subducting plate (Fig. 11).

LITHOSPHERIC STRESS ANALYSIS

We employed three-dimensional finite element models

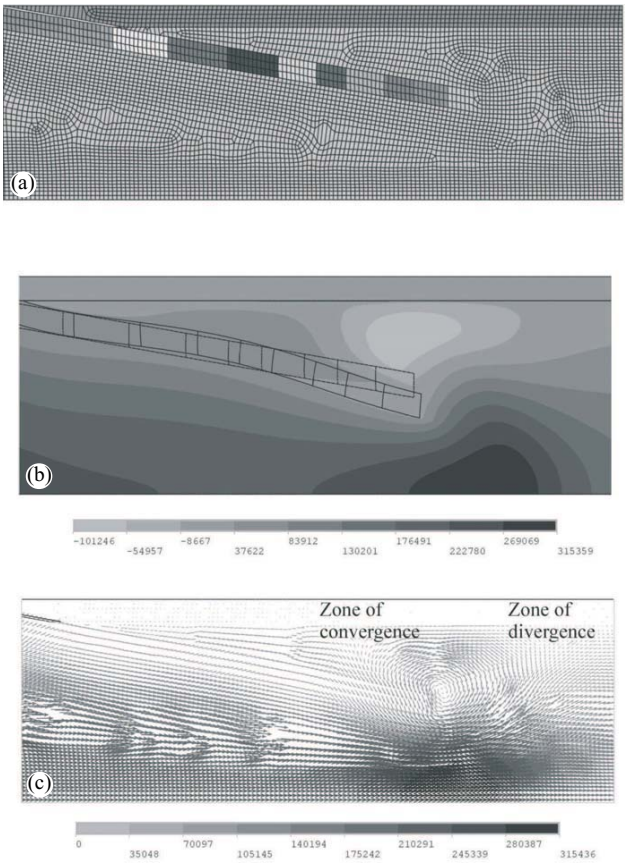

Fig.9. Type 2 experiments with lithospheric slab of varying density, subducting into mantle of uniform density. **(a)** Initial 2D FE model illustrating mesh structure of a lithospheric plate of varying density, as shown by blocks of different shades **(b)** Shade contours illustrating the distribution of horizontal displacement in the flow. Contours with negative values marks region of flow against the subduction direction. **(c)** Displacement vectors around the subducted slab. Note the zones of secondary flow convergence and divergence on either side of a vortex in the mantle wedge.

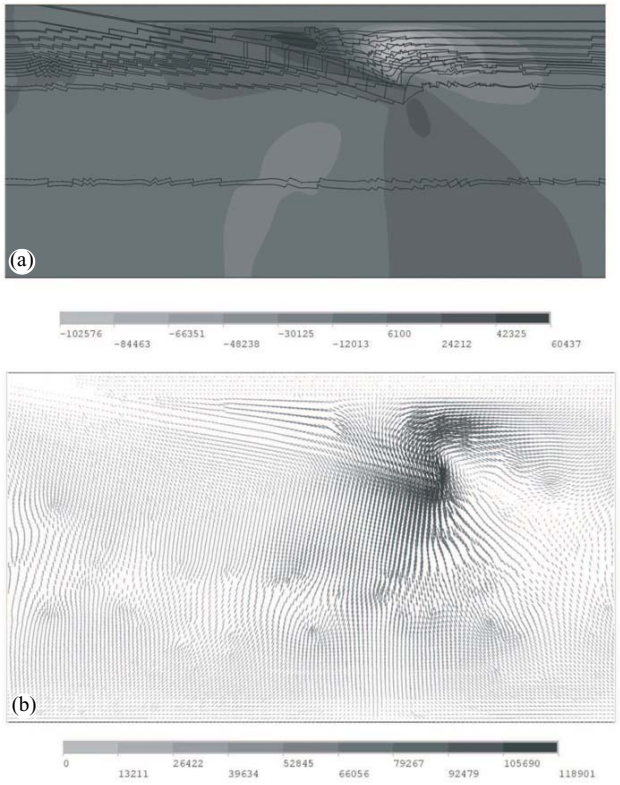

Fig.10. Type 2 experimental models with varying densities in both lithosphere and mantle. **(a)** Distribution of horizontal flow displacements. **(b)** Flow patterns around the slab, characterized by a secondary convergence below the overriding plate. Horizontal lines in the models indicate density stratifications. Corresponding values are described in Table 1.

to analyze the distribution of lithospheric stresses as a function of the geometry and the kinematics of plate subduction. Type 2 experimental conditions were employed to investigate the nature of lithospheric stresses distribution on either side of subduction zones. The lithospheric plate had a density variation, and underwent a flexural deformation, as described in the previous section during the subduction. A set of experiments was performed by varying initial subduction inclination (α), keeping all other parameters constant.

We mapped horizontal normal stresses in convergent zones. The stress maps revealed distinct belts of horizontal compression and tension in the lithospheric plates. Their lateral extents vary with the initial subduction angle. For $\alpha = 5^o$, horizontal compression localizes in the overrding plate at a distance of 800 – 1000 km from the trench line (Fig.12a). This zone is much wider compared to the lithospheric thickness. The compression zone is paired with a belt of horizontal tension, which is located towards the trench line. The two stress belts have nearly equal widths. However, the magnitude of tensile stresses is much lower than (10^{-2}) that in the compression belt. There is a zone of intense horizontal compression close to the trench line in the subducting plate. This secondary compression zone is narrow in width compared to that in the overriding plate. The overriding and the subducting plates have global tensile and compressive stresses. However, the stress magnitudes are low.

With increase in subduction angle the stress distributions change significantly, both in magnitude as well as their lateral extent. For $\alpha = 10^o$, the compression zone becomes narrow, and lies above the line of maximum flexure on the lithospheric slab (Fig. 12b). A narrow belt of large tensile stresses develops along the line of subduction. Its magnitude is almost equal to that of the compression zone. This type

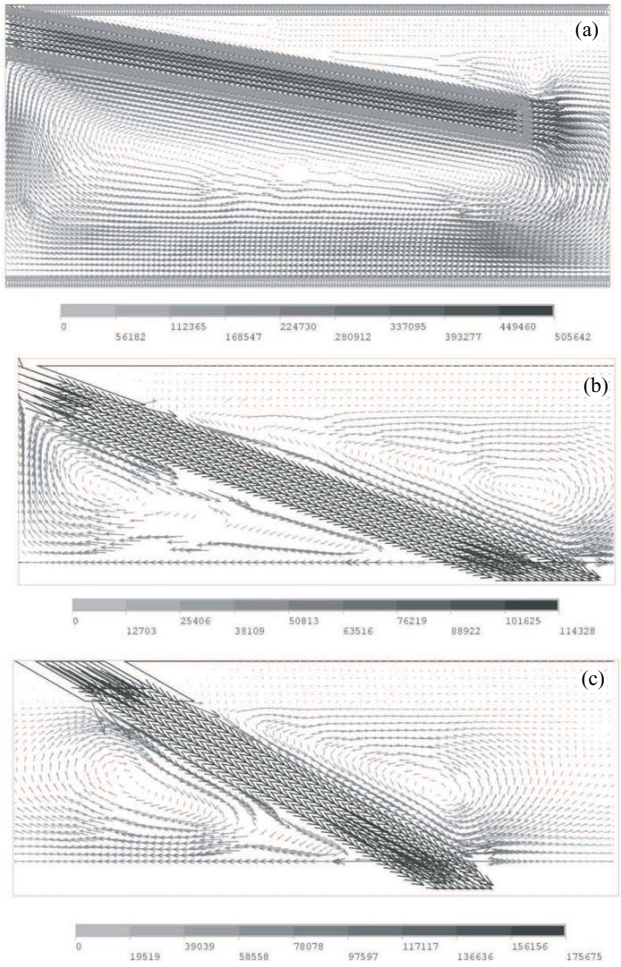

Fig.11. Flow induced by detached lithospheric plate subducting in mantle with uniform density. **(a)** $\alpha = 10°$, **(b)** $\alpha = 20°$ and **(c)** $\alpha = 30°$.

of stress localization occurs along the hinge line of flexed elastic bar. There is also a significant change in the global lithospheric stress field far away from the line of subduction. In the previous model with $\alpha = 5^o$ the overriding and the subducting lithospheric plates have contrasting global stress fields; one with tension and the other with compression (Fig. 12a). For $\alpha = 10^o$, the two plates show similar global stress fields characterized by weak tensile stresses (Fig. 12b).

With further increase in subduction angle ($\alpha = 16^o$) the compression belt in the overriding plate remains virtually unchanged. However, the adjoining tensile stress regime close to the subduction line becomes narrow in width. On the other hand, the tensile stress belt lying along the hinge line of subduction has a relatively large width. Increasing α greatly influences the global stress fields (Fig. 12c). Both the overriding and the subducting plates have tensile stresses, but with contrasting magnitudes. The subducting plate remains under much larger tensile stresses compared to the overriding plate.

Some examples can be cited from natural trenches to discuss the stress fields obtained from numerical models. The overriding plate in the Izu arc, 33°N shows crustal thickening over a broad zone, which is located away from the trench line (Fig. 13a; Stern 2002). The geographical disposition can be compared with the compressional stress field observed in the finite element models (Fig. 13a). Horizontal extent of the thickened crust depends on the subduction angle. Compared to the Izu arc, the Eastern Aleutian Arc has a larger subduction angle, and the overriding plate shows large amounts of crustal thickening in relatively narrow regions (Fig. 13b). This contrasting crustal thickening can be explained, at least qualitatively, by using the lithospheric stress models (Fig. 12). For a low

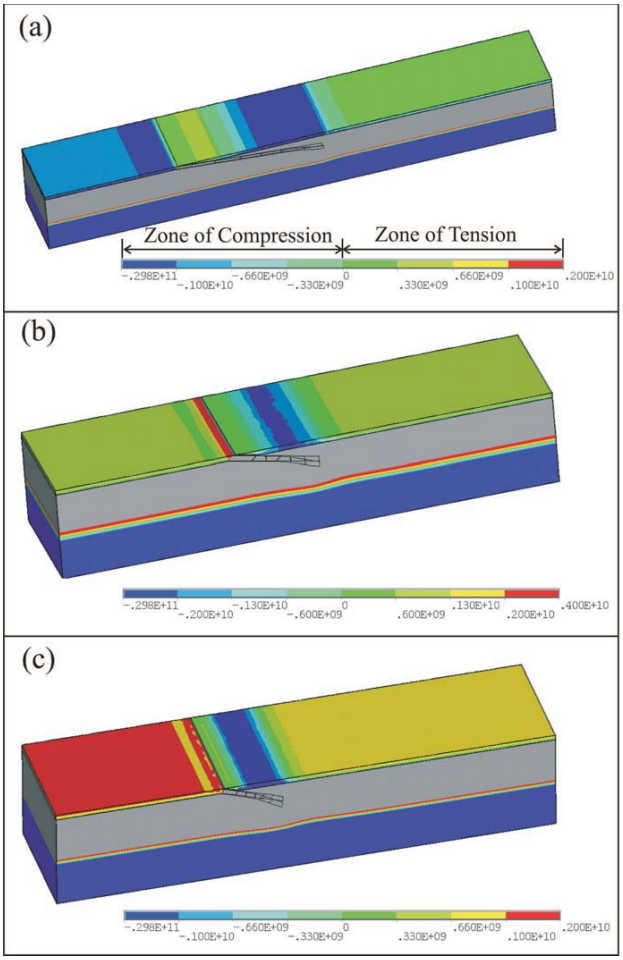

Fig.12. Lithospheric stress distributions in convergent zones obtained in Type 2 experiments. **(a)** $\alpha = 5^o$, **(b)** $\alpha = 10^o$ and **(c)** $\alpha = 16^o$. Colour contours show horizontal stress components, where positive and negative values indicate tensile and compressive stress components, respectively.

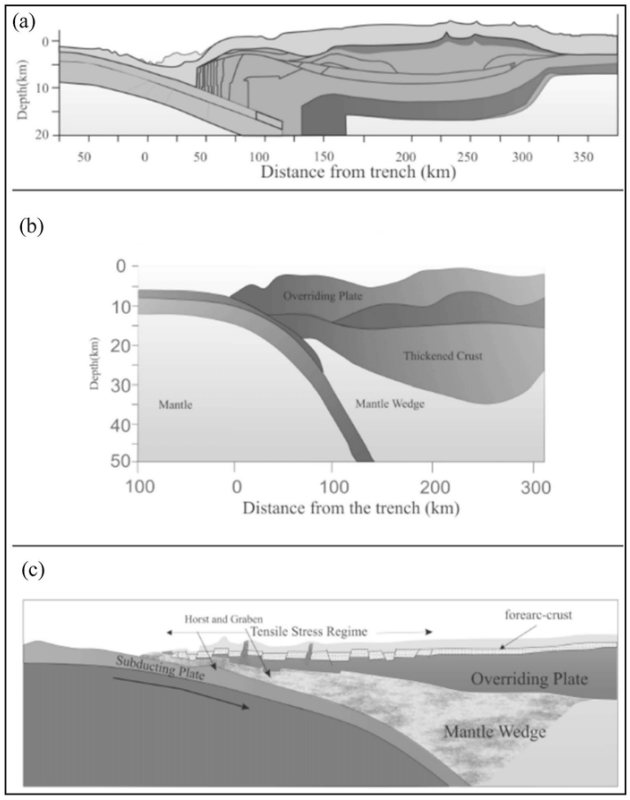

Fig.13. (a) and **(b)** are geological sections of Izu Arc, 33N and eastern Aleutian Arc respectively both of which have varying subduction angles. **(c)** Extensional faults revealing the tensile stress belt in a non-accretionary fore-arc (*after* Stern et al. 2002).

subduction angle, the compression zone has a large width, which becomes narrow with increasing subduction angle. The Izu arc has low subduction angle (~ 8°), whereas the Aleutian arc has a relatively large subduction angle (~ 45°). Convergent tectonic regimes often have fore-arc settings that may be either of accretionary or non-accretionary type (Stern 2002). The latter show extensional deformation in the frontal part of the overriding plate, which is indicated by the development of normal fault sequences (Fig.13c). The crustal structures imply a tensile stress field as obtained from numerical models (Fig.12).

DISCUSSION

Our FE model experiments show that the patterns of mechanical flow in subduction zones depend largely on the nature of plate motion. Translational movement produces a vortex in the mantle wedge, which is replaced by a secondary flow convergence when the slab undergoes density-controlled flexural bending. This kinematic analysis has an implication in studying tectonic evolution of convergent belts. For example, the Himalayan convergent system is believed to have evolved by steepening of the subducting lithospheric slab, implying flexure bending at a later stage (Leech et al. 2005). During the phase of translation plate motion, the Himalayan subduction involved southward flow in the mantle beneath the Tibetan plateau. According to our analysis, there might have been flow reversal, and the southward flow was replaced by northward one, as the subducting plate began to steepen its dip by flexural movement.

In order to simulate density-controlled lithospheric flexure, we considered models with and without density variation in the mantle. Uniform mantle-density models aim at studying a specific case where the density contrast between lithospheric plate and the ambient mantle is very large and lithospheric flexure takes place mostly by the effect of density gradient in the lithospheric plate. This type of models is certainly idealistic in nature. Geological and geophysical studies suggest that the mantle density does vary with depth significantly (Ganguly et al. 2008). Secondly, the density contrast can be of different magnitudes in different subduction zones. Again, several workers have proposed that the lithospheric plate may be less dense compared to the mantle in the deeper level (Fukao et al. 1992, 2001; van der Hilst, 1995). The lithospheric plate thus remains under positive buoyancy, and cannot move or flex downward. It has been shown that the lithospheric plate has a tendency to move laterally in the horizontal direction. In contrast, Ganguly et al. (2008) have demonstrated that a subducting lithospheric slab is likely to have net negative buoyancy even after crossing the transition zone. It follows from this discussion that plate subduction can be driven under varying buoyancy forces, the effects of which require further studies.

In this study we have dealt with mantle flow resulting from only the mechanical interaction between subducting lithospheric slabs and the mantle medium. It is a well-known fact that the mantle has a global convection flow, which was not considered in our modeling. Evidently, different flow patterns presented in the preceding sections do not reflect the actual flow field in the mantle. This analysis principally demonstrates how the global kinematic state can be perturbed by the mechanical movement of a lithospheric slab. In order to obtain the total flow field, we need to superimpose the perturbed field on the global flow field. Thermo-mechanical processes can take place also locally in different ways, leading to additional complexities in the flow pattern. For example, fluid materials released from the subducting lithosphere fluxes heat into the mantle wedge, producing a secondary convection cell (Turcotte

and Schubert, 2002; Bose and Ganguly, 1998). Our experiments reveal that vortex-type flow can be generated in the mantle wedge due to the mechanical movement of the lithospheric plate. Evidently, the resultant flow in the mantle wedge can be extremely complex due to interferences of flows induced by thermo-mechanical effects and the plate movement.

CONCLUSIONS

Based on the experimental findings, we arrive at the following conclusions.

1. A lithospheric slab undergoing translational movement develops flow separations in the mantle wedge, forming a vortex-like flow pattern in the mantle wedge, irrespective of both subduction angle and subduction rate. Typical open streamlines characterize large-scale flow patterns beneath the subducting lithospheric plate when the subduction angles are low. This pattern is replaced by vortex with increasing subduction angles. The vortex geometry is a function of subduction rate. With a decrease in subduction rate it tends to enlarge in size, and shift away from the subducting plate.
2. Pure flexural (rotational) motion of the plate induces a back flow in the mantle wedge, and a subduction-ward flow beneath the moving plate. For a combination of rotation and translation, the latter shows separation, and develops a back flow.
3. The geometry of density-controlled lithospheric flexure depends on the mantle density variation with depth. For a uniform mantle density, the flexure deflection is non-uniform, and turns to be relatively uniform when the mantle density increases with depth.
4. Density-controlled flexure gives rise to secondary flow convergence below the overriding plate.
5. Detached lithospheric slabs produce symmetrically disposed vortices, the shape of which varies with subduction angle.
6. Lithospheric stresses in the overriding plate show localization of tensile and compression regimes close and away from the trench line respectively. The subducting lithospheric plate is under far-field compressive stresses, which is replaced by tensile stresses with increasing subduction angle.

It may be noted that model results presented in this paper are based on a number of simplistic assumptions, which adhere to some limitations. (a) To simulate the lithosphere and the underlying mantle medium, we have used a two-layer mechanical model, consisting of two units with contrasting viscosities that remain constant in space and time. However, the mantle has a varying viscosity with depth, whereas the lithosphere can change its viscosity during the subduction (e.g. Tirone et al. 2009). The viscosity contrast can therefore change with progressive movement. (b) The transition zone is likely to act as a mechanical layer owing to its viscosity and density contrasts with the upper and lower mantle. This layer can give rise to an additional effect on the movement of lithosphere and thereby the flow pattern. (c) This study presents an analysis of flow patterns for initial stages of lithospheric plate subduction. The process is likely to be complex due to large modifications of plate geometry in the advance stages.

Acknowledgements: We thank Prof. Jibamitra Ganguly and an anonymous reviewer for their critical comments on an early version of the manuscript. Dr. Manish Mamtani is gratefully acknowledged for his editorial help. We thank Amiya Baruah and Kaustav Chatterjee for their help in diagram preparations.

References

Bose, K. and Ganguly, J. (1995) Experimental and theoretical studies of the stabilities of talc, antigorite and phase A at high pressures with application to subduction processes. Earth Planet. Sci. Lett., v.136, pp.109-121.

Chemenda, A.I., Burg, J-.P. and Mattauer, M. (2000) Evolutionary model of the Himalaya-Tibet system: geopoem based on new modeling, geological and geophysical data. Earth Planet. Sci. Lett., v.174, pp.397-409.

Davies, G. (1995) Penetration of plates and plumes through the mantle transition zone. Earth Planet. Sci. Lett. v.133, pp.507-516.

Davies, G.F. (1999) Dynamic Earth, Cambridge, 458p.

Forsyth, D. and Uyeda, S. (1975) On the relative importance of the driving forces of plate motion. Geophys. Jour. Internat., v.43, pp.163-200.

Fukao, Y., Widiyantoro, S. and Obayashi, M. (2001) Stagnant Slabs in the Upper and Lower Mantle Transition Region. Reviews of Geophysics, v.39, pp.291-323.

Fukao, Y., Obayashi, M., Inoue, H. and Nenbai, M. (1992) Subducting slabs stagnant in the mantle transition zone. Jour. Geophys. Res., v.97, pp.4809-4822.

Ganguly, J., Freed. A.M. and Saxena, S.K. (2008) Density profiles of oceanic slabs and surrounding mantle: Integrated thermodynamic and thermal modeling, and implications for the fate of slabs at the 660 km discontinuity. Physics Earth Planet. Int., doi:10.1016/j.pepi.2008.10.005.

GERYA, T.D., YUN ,D.A. and SEVRE, E.O.D. (2004) Dynamical Causes for incipient magma chambers about slabs. Geology, v.32, pp.89-92.

GRAND, S.P., VAN DER HILST, R.D. and WIDIYANTORO, S. (1997) Global seismic tomography: a snapshot of convection in the Earth. GSA Today, v.7, pp.1-7.

HAGER, B.H. (1984) Subducted slabs and the geoid: constraints on mantle rheology and flow. Jour. Geophys. Res., v.89, pp.6003-6015.

HONDA, S. (2009) Numerical simulations of mantle flow around slab edges. Earth Planet Sci Lett., v.277, pp.112-122.

HOUSEMAN, G.A. and GUBBINS, D. (1997) Deformation of subducted oceanic lithosphere. Geophys. Jour. Int., v.131, pp.535-551.

LEECH, M.L., SINGH, T.S., JAIN, A.K., KLEMPERER, S.L. and MANICKAVASAGAM, R.L. (2005) The onset of India–Asia continental collision: Early, steep subduction required by the timing of UHP metamorphism in the western Himalaya. Earth Planet. Sci. Lett., v.234, pp.83-97.

LOWRIE, W. (2007) Fundamentals of Geophysics (2nd Edition) Cambridge University Press, 381p.

MANDAL, N., SAMANTA, S.K. and CHAKRABORTY, C. (2001) Numerical modeling of heterogeneous flow fields around rigid objects with special reference to particle paths, strain shadows and foliation drag. Tectnophysics, v.330, pp.177-194.

MASUDA, T. and ANDO, S. (1988) Viscous flow around arigid spherical body: a hydrodynamical approach. Tectnophysics, v.148, pp.337-346.

PYSKLYWEC, R.N. and ISHII, M. (2000) Time dependent subduction dynamics driven by the instability of stagnant slabs in the transition zone, Physics Earth Planet. Int., v.149, pp.115-132.

PYSKLYWEC, R.N. and MITROVICA, J.X. (1998) A mantle flow mechanism in the long-wavelength subsidence of continental interiors. Geology, v.26, pp.687-690.

RANALLI, G. (1987) Rheology of the Earth. Allen & Unwin, London, 365p.

RINGWOOD, A.E. (1994) Role of the transition zone and 660 km discontinuity in mantle dynamics. Phys. Earth Planet. Int., v.86, pp.5-24.

STERN R.J. (2002) Subduction Zones, Reviews of Geophysics, v.40(4), pp.3.1-3.38,

TACKLEY, P.J. (1996) On the ability of phase transitions and viscosity layering to induce longwavelength heterogeneity into the mantle. Geophys. Res. Lett., v.23, pp.1985-1988.

TIRONE, M., GANGULY, J. and MORGAN, J.P. (2009) Modelling petrological geodynamics in the Earth's mantle. Geochemistry, Geophysics, Geosystems, 10, doi:10.1029/2008GC002168.

TURCOTTE, D.L., SCHUBERT G. and Olson, P. (2004) Mantle Convection in the Earth and Planets (4th Edition) Cambridge University Press, 940p.

TURCOTTE, D.L. and SCHUBERT, G. (2002) Geodynamics(2nd Edn), 456p.

VAN DER HILST, R. (1995) Complex morphology of subducted lithosphere in the mantle beneath the Tonga trench. Nature, v.374, pp.154-157.

VAN DER HILST, R.D., ENGDAHL, E.R., SPAKMAN, W. and NOLET, G. (1991) Tomographic imaging of subducted lithosphere below northwest Pacific island arcs. Nature, v.353, pp.37-43.

WEINS, D.A. and GILBERT, H.J. (1996) Effect of slab temperature on deep-earthquake aftershock productivity and magnitude-frequency relations. Nature, v.384, pp.153-156.

ZHONG, S. and GURNIS, M. (1994) Role of plates and temperature dependent viscosity in phase change dynamics. Jour. Geophys. Res., v.99, pp.15903-15917.

(Received: 8 March 2009; Revised form accepted: 12 June 2009)